CHAPTER 3

PROPAGATION OF LOCALIZED WAVES IN COLLISIONLESS PLASMA MEDIA

3.1. Introduction

Most of the previous studies [1,5,24,25] have dealt solely with the propagation and generation of LW pulses in free space. In this chapter we extend our investigation to the characteristics of LW propagation through dispersive media. These media may be modeled by the Klein-Gordon equation [142]. Our approach utilizes a spectral analysis [109] that focuses on the depletion of the Fourier spatio-temporal components as the radiated LW pulses propagate away from their dynamic sources. In this work, we shall demonstrate that contrary to our initial expectation the depletion of the spectral components of the dispersive Klein-Gordon field may become slower than that associated with the free scalar field. This means that we can design a LW pulse that exhibits a slower decay rate as it propagates in a dispersive medium than in free space. It will be shown that this behavior results from the proper tuning of the coupling of the spatio-temporal components of the excitation wavefield to the plasma frequency ω_p characterizing the dispersive medium.

3.2. Formulation of the Radiated Field

Consider the 3D Klein-Gordon equation modeling the propagation of waves in a collisionless plasma medium, viz.,

$$\nabla^2\Psi(\mathbf{r},t)-\frac{1}{c^2}\frac{\partial^2}{\partial t^2}\Psi(\mathbf{r},t)-\frac{\omega_p^2}{c^2}\Psi(\mathbf{r},t)=0, \tag{3.2.1}$$

where $\omega_p = 2\pi f_p$, f_p being the plasma frequency. In analogy to the scalar wave equation field, we assume to have a dynamic aperture source situated at $z = 0$ and illuminated by the azimuthally symmetric initial wavefield

$$\Psi(\rho, z = 0, t) = \Re\left(\hat{\Psi}(\rho, z = 0, t)\right), \tag{3.2.2a}$$

where

$$\hat{\Psi}(\rho, z = 0, t) = \left\{ \frac{1}{2\pi} \int_0^\infty d\chi \chi J_0(\chi\rho) \int_0^\infty d\omega\, \Phi(\chi, \omega)\, e^{i\omega t}\, e^{-i\sqrt{(\omega/c)^2 - \chi^2 - k_p^2}\, z} \right\}_{z=0}. \tag{3.2.2b}$$

Here, ω is the Fourier radial frequency variable, $\chi = \sqrt{k_x^2 + k_y^2}$ is the transverse spatial Fourier variable and $k_p = \left(\omega_p / c\right)$. To generate a time-limited, nonseparable localized wave, the Fourier spectrum $\Phi(\chi, \omega)$ is chosen as [5,99,109,127]

$$\Phi(\chi, \omega) = \frac{T}{4\pi^{1/2}} e^{-\chi^2 a/4\beta}\, e^{-T^2\left(\omega - \left(\left(\chi^2 + k_s^2\right)/4\beta\right)c - \beta c\right)^2}. \tag{3.2.3}$$

The parameter T controls the width of the Gaussian time window applied to turn off the excitation wavefield. It should be noted that the argument of the spectral Gaussian ω window couples the temporal frequency variable ω to the spatial spectral variable χ. The same argument depends on a characteristic source frequency denoted by k_s. In Sec. 3.3, it will be shown that an unusual decay behavior is exhibited by LW pulses propagating in dispersive media when k_s is tuned to a value close to the plasma frequency k_p. This necessarily requires an *a priori* knowledge of the plasma frequency of the medium and that the functional dependence of the ω-χ coupling should incorporate such a frequency. In the limit $T \to \infty$, the excitation time of the dynamic source, as well as its size, become infinite and the Fourier spectrum given above reduces to the singular function

$$\Phi(\chi, \omega) = \frac{1}{4} e^{-\chi^2 a/4\beta}\, \delta\left(\omega - \left(\left(\chi^2 + k_s^2\right)/4\beta\right)c - \beta c\right). \tag{3.2.4}$$

Even though the above Fourier spectrum leads to physically unrealizable situations involving apertures of infinite sizes, it is useful in deriving explicit expressions for the spatial and temporal spectra [99,106] under the condition that the width of the spectral ω window is much smaller than the bandwidth of the temporal frequency spectrum.

In analogy to LW pulses launched in free space, we can apply Huygens' construction to obtain the following formula for the Klein-Gordon field generated from a flat dynamic aperture situated at the $z = 0$ plane:

$$\hat{\Psi}(\rho,z,t) = \frac{1}{2\pi}\int_0^\infty d\chi\chi J_0(\chi\rho)\int_0^\infty d\omega\,\Phi(\chi,\omega)\,e^{i\omega t}\,e^{-i\sqrt{(\omega/c)^2-\chi^2-k_p^2}\,z}. \tag{3.2.5}$$

The details of the derivation of this representation of the radiated field are provided in Appendix 3-A. For an infinite-time excitation, we substitute the singular spectrum given in Eq. (3.2.4) and carry out the integration over ω to obtain

$$\hat{\Psi}(\rho,z,t) = \frac{1}{8\pi}\int_0^\infty d\chi\chi J_0(\chi\rho)\,e^{-\chi^2 a/4\beta}\,e^{i\left(\beta+\left(\chi^2+k_p^2+\Delta_{sp}\right)/4\beta\right)ct}\;e^{i\sqrt{\left(\beta-\left(\chi^2+k_p^2+\Delta_{sp}\right)/4\beta\right)^2+\Delta_{sp}}\,z}. \tag{3.2.6}$$

Here, $\Delta_{sp} \equiv k_s^2 - k_p^2$ indicates the deviation of the square of the characteristic frequency k_s from that of the plasma frequency k_p. The former is related to the spectral content of the source while the latter is a property of the medium. One should note that for the special case when $k_s = k_p$, Eq. (3.2.6) reduces to

$$\hat{\Psi}(\rho,z,t) = \frac{1}{8\pi}\int_0^\infty d\chi\chi J_0(\chi\rho)\,e^{-\chi^2 a/4\beta}\,e^{i\left(\beta+\left(\chi^2+k_p^2\right)/4\beta\right)ct}\;e^{i\left(\beta-\left(\chi^2+k_p^2\right)/4\beta\right)z}. \tag{3.2.7}$$

In contradistinction to the scalar Focus Wave Mode (FWM) [99,106,107] radiated from a dynamic aperture into free space, the above expression does not contain any backward propagating components as long as $k_p > 2\beta$. The integration over χ can be evaluated explicitly, yielding the following radiated wavefield:

$$\hat{\Psi}(\rho,z,t) = \frac{\beta}{4\pi(a+i(z-ct))} e^{-\beta\rho^2/(a+i(z-ct))} e^{i\beta(z+ct)} e^{-ik_p^2(z-ct)/4\beta}. \qquad (3.2.8)$$

The field radiated from an infinite aperture for the case when $k_s = k_p$ is shown in Fig. 3.1a. The real part of the expression given in Eq. (3.2.8) is plotted for $a = 0.00001$ m, $\beta = 1..25$ m^{-1} and $z = 236.25$ m. It is interesting to determine how the LW field behaves when k_s is different from k_p. This allows us to check the robustness of the LW pulses generated in a dispersive medium. The real part of Eq. (3.2.6) is plotted in Fig. 3.1b for $k_s = 1.02k_p$ at $z = 236.25$ m for the same parameter values used earlier. One should note that, as k_s differs from k_p, the radiated pulse loses its symmetric form and more oscillations are introduced into its trailing edge. In contradistinction, the leading portion of the pulse, is cutoff more quickly. This behavior is illustrated in Fig. 3.2 by comparing the axial ($\rho = 0$) dependence of the radiated wavefield for $k_s = 1.02k_p$ and $k_s = 1.05k_p$ to the $k_s = k_p$ case.

To investigate the decay properties of the centroid of the LW field radiated from a finite-time dynamic aperture, we have evaluated numerically the amplitude of the field given in Eq. (3.2.5) using the finite-time spectrum in Eq. (3.2.3), with $k_s = k_p$, and substituting for the parameters involved the values $a = 0.00001$ m, $\beta = 1..25$ m^{-1} and $cT = 6.25$ m. Such parameter values might not be physically suitable for all applications; however, they have been adopted in order to compare our results to previous studies. Other choices of parameters suitable for different kind of applications are also possible. Figure 3.3 compares the decay of the centroid ($z = ct$ and $\rho = 0$) amplitudes of LW pulses radiated in media characterized by different plasma frequencies. Specifically, we have used the values $f_p = 0,\ 20,\ 30$ GHz, the first case corresponding to propagation in free space. It can be seen from this figure that there is a clear slow down in the decay rate of the amplitude of the propagating LW pulses as the plasma frequency characterizing the

medium is increased. In the next section, we provide an explanation for this unanticipated result. We argue that this unusual behavior is a consequence of the distinct mechanism of the depletion of the spectral components of LW pulses as they propagate away from their source plane [109].

3.3. Depletion of the Spectral Components

In earlier studies of LW pulses launched from dynamic apertures into free space [109,110], it has been shown that the amplitude of the centroids of their wavefields decreases with distance due to a particular depletion of the spectral content of the pulses. The difference between the spectral loss of LW pulses and that of the more familiar quasi-monochromatic signals is a result of the unique coupling between the spatial and temporal frequency components of the radiated LW fields [109]. To have a better understanding of the aforementioned depletion mechanism, we rewrite the radiated LW field given in Eq. (3.2.5) as

$$\hat{\Psi}(\mathbf{r},t)=\int_0^\infty d\chi\chi J_0(\chi\rho)\Phi_s(\chi,z,t)\,, \tag{3.3.1a}$$

where $\Phi_s(\chi,z,t)$ is the transverse spatial frequency spectrum. For the finite-time excitation based on the spectrum in Eq. (3.2.3), the spatial spectrum is given explicitly as

$$\Phi_s(\chi,z,t)=\frac{T}{8\pi^{3/2}}\int_0^\infty d\omega e^{-\chi^2 a/4\beta}\, e^{-T^2\left(\omega-\left(\left(\chi^2+k_s^2\right)/4\beta\right)c-\beta c\right)^2}\, e^{i\omega t}\, e^{-i\sqrt{(\omega/c)^2-\chi^2-k_p^2}\,z}\,. \tag{3.3.1b}$$

The decay of the center of the pulse is controlled primarily by the Gaussian ω window which is centered around $\left[\left(\left(\chi^2+k_s^2\right)/4\beta\right)+\beta\right]$. We know from previous studies of the depletion of the spectral components of LW pulses [109] that the oscillations introduced with distance into the ω windows are smaller in number for the windows centered around the higher frequency components. We also know that the same oscillations increase inside

all ω windows centered around the significant χ components as the pulse travels away from the source plane. However, the rate at which these oscillations are introduced into the spectral windows is much slower for higher χ values than for lower ones. The integration over these oscillations, as indicated in Eq. (3.3.1b), results in the annulment of the contributions of the windows containing large number of cycles. As a consequence, the χ values around which such spectral windows are centered provide negligible contributions to the amplitude of the center of the LW field when the integration over χ in Eq. (3.3.1a) is carried out. Thus, the low spatial spectral components are depleted first as the pulse propagates forward in the dispersive medium.

In contradistinction to the case of LW pulses radiated into free space, the presence of the additive term $k_s^2/4\beta$ in the argument of the Gaussian ω window results in effectively placing the centers of the ω windows at higher frequencies. Thus, the presence of the $k_s^2/4\beta$ term results in delaying the spectral depletion of various χ components to farther distances. As a consequence, the decay of the centroid of the Klein-Gordon LW pulse is significantly reduced when compared to the case of a scalar LW pulse traveling in free space. In Figs. 3.4.a-d, the depletion of the spectral content is compared to that of free space for various plasma frequencies, with the source frequency k_s equal to k_p. In these figures we display the initial spatial frequency content at $z = ct = 0$, together with the depleted spectra at $z = ct = 236.25$ and 472.5 m. The figures compare the depleted spectral content of the field propagating in plasma and in free space. They are plotted for plasma frequencies $f_p = 10,$ 20, 30 and 40 GHz. It is clear that the depletion of the spatial spectral content is slowed down as the plasma frequency is increased. According to Eq. (3.3.1a) the integration of these curves over χ yields the amplitude of the centroid ($\rho = 0$ and $z = ct$) of the LW pulse. As a consequence, the decay rate of the amplitude of

the LW pulse is decreased as the plasma frequency of the medium is increased, as long as the characteristic frequency of the source is set equal to k_p.

Another spectral property that the Klein-Gordon LW pulses have is that their lower cutoff frequencies are dependent on the plasma frequency. This is understood if one refers to the temporal frequency content defined as

$$\Phi_t(\rho,\omega) = \int_0^\infty d\chi\chi J_0(\chi\rho)\Phi(\chi,\omega). \tag{3.3.2}$$

Substituting the spectrum given in Eq. (3.2.4) and setting $k_s = k_p$, we obtain

$$\Phi_t(\rho,\omega) = \frac{\beta}{2c} J_0\left(\sqrt{4\beta(\omega/c) - 4\beta^2 - k_p^2}\,\rho\right) e^{-\left((\omega/c)-\left(k_p^2/4\beta\right)-\beta\right)a} \mathrm{H_s}\left((\omega/c)-\left(k_p^2/4\beta\right)-\beta\right), \tag{3.3.3}$$

where $\mathrm{H_s}$ is the Heaviside unit step function. Clearly, the parameter *a* controls the upper temporal frequency limit. The term $k_p^2/4\beta$ in the argument of the unit step function will move the lower cutoff frequency to a higher value. For $k_p >> 2\beta$, the lower frequency limit will move up significantly. In the finite-time excitation scheme, the lower frequency components are depleted first as the distance *z* is increased. As a consequence, the initial decay of the centroid of the launched LW pulse should be slower. Furthermore, such a pulse traveling in a dispersive medium would have a deeper focused depth in the near-to-far field range than an equivalent pulse propagating in free space. This is achieved by properly tuning the excitation wavefield so that the parameter k_s is chosen to be equal to the plasma frequency k_p defining the dispersion of the medium.

3.4. Practical Considerations

For large f_p, the maximum frequency of the temporal spectrum might move to higher values. We usually define $\omega_{\max}$ as the point at which the exponential term on the right

hand side of Eq. (3.3.2) decays to its $\left(e^{-4}\right)$ value [109]. For free space this criterion yields $\left(\omega_{\max}/c\right)=4/a$. In the case where $f_p=10$ GHz, it follows that $\left(k_p^2/4\beta\right)=8773\text{m}^{-1}$ $>>\beta$. Even though this will raise $\omega_{\min}$, it will have a very slight influence on $\left(\omega_{\max}/c\right)$, which equals $\left(4/a\right)=400000\ \text{m}^{-1}$ for free space. It must be emphasized, however, that the slight increase in the bandwidth of the pulse to 408773 m^{-1} does not cause the observed decrease in the decay rate displayed in Fig. 3.3. A free space LW pulse having this slightly larger bandwidth does not exhibit the same slow decay of the Klein-Gordon LW pulse. On the other hand, one should be more careful when dealing with larger values of f_p. For example, when $f_p=40$ GHz, the quantity $\left(k_p^2/4\beta\right)=140368\ \text{m}^{-1}$ is comparable to $\left(4/a\right)$. Taking into consideration that $\omega_{\min}$ has moved up very closely to the $\left(4/a\right)$ point, we anticipate that the $\left(e^{-4}\right)$ point will shift up to higher values. A brief calculation yields the upper cutoff frequency $\left(\omega_{\max}/c\right)=540368\ \text{m}^{-1}$. There is a significant increase here in the bandwidth of the LW pulse due to the tuning of its spectral coupling to the plasma frequency. Such an increase in the bandwidth definitely contributes to the slow down in the depletion of the spectral content.

At this point, it is worthwhile to investigate the possibility of having $k_s\neq k_p$. Toward this end, the integration given in Eq. (3.3.1) is evaluated at $z=236.25$ m. Fig. 3.5a displays the axial time dependence of the amplitude of the highly focused central portion of the pulse (at $\rho=0$). In this figure, the amplitudes of the LW pulses are plotted for the tuned cases, when $k_s=k_p=0$ and $k_s=k_p=209.4\,\text{m}^{-1}$, as well as for the case when $k_s=1.02\,k_p$. All amplitudes are normalized with respect to the peak of the plasma wavefield for $k_s=k_p$. It can be seen that the centroid of the LW pulse traveling in plasma

is larger than that of a pulse propagating in free space. Similarly to the wavefields radiated from infinite apertures [cf. Figs. 3.2 and 3.3], one should observe that the finite-time LW pulses lose their symmetric forms for $k_s \neq k_p$. Furthermore, the peaks of the pulses traveling in a plasma become smaller than those in free space. At farther distances, the relative amplitude of the three wavefields (corresponding to the values $k_s = k_p = 0$, $k_s = k_p = 209.4\ \mathrm{m}^{-1}$ and $k_s = 1.02 k_p$) remains unchanged. This is shown in Fig. 3.5b for $z = 708.74\ \mathrm{m}$. It is clearly seen that the deterioration in the detuned case occurs primarily in the region near the source plane. At larger distances, the relative strength of the amplitudes of the three pulses does not change. This demonstrates the critical dependence of the decay behavior of Klein-Gordon LW pulses on the tuning of the spectral quantity k_s to the plasma frequency. However, such a dependence is primarily a near-field behavior and does not affect the relative decay of the centroid of the LW pulse as it travels away from the aperture. Finally, we would like to emphasize that the extremely high plasma frequencies adopted in this chapter have been chosen to clearly illustrate the slowing down of the decay of the centroid of the LW pulse.

For lower plasma frequencies, we have essentially the same robustness. For example, if the same LW pulses were propagated through the ionosphere ($f_p = 6 - 28\ \mathrm{MHz}$), the decay patterns in free space and the ionospheric plasma would be indistinguishable as long as k_s equaled k_p. For $k_s \neq k_p$, LW pulses traveling in the ionosphere undergo an initial fast decay. At larger distances, they exhibit decay rates comparable to LW pulses traveling in free space.

3.5. Concluding Remarks

In this chapter, we have demonstrated that LW pulses propagating in dispersive media display unusual decay patterns. This is especially true when the source spectral parameter

k_s is tuned to the plasma frequency k_p of the medium. Under this provision, the radiated LW pulses exhibit decay rates slower than those characterizing analogous LW pulses traveling in free space. This slow decay rate is attributed to the extraordinary depletion of the spectral components of LW pulses as the latter travel away from their source plane [109]. Unlike quasi-monochromatic signals, the depletion of the spectral components of the carrier-free ultra-wideband LW pulses is controlled by the coupling between the spatial and temporal spectral components. For the LW pulses studied in this chapter such a coupling includes the k_s parameter. The existence of this spectral parameter effectively places the ω windows scanning the spatial spectrum at higher values. As a consequence, the depletion of the spectral components is reduced. This results in a reduction of the decay rate of the centroid of the Klein-Gordon LW wavefield.

Tuning the spectral parameter k_s to the plasma frequency k_p requires *a priori* knowledge of the plasma frequency of the medium. In a practical situation, we may not be able to completely tune k_s to equal k_p. For this reason, we have investigated the situation when $k_s \neq k_p$ and have found that, except for small deviations, the decay of a LW pulse is as slow as in the tuned case. The pulse, however, loses its symmetrical form along the direction of propagation ($\rho = 0$). For $k_s > k_p$, the forward edge of the pulse dies off quickly, while the trailing portion develops oscillations and becomes more extended. The decay rate of the centroid of the pulse is comparable to that of the tuned case, apart from a slightly faster rate of decay exhibited at short distances. This causes the centroid to have a smaller amplitude than the tuned case. However, once the two pulses start to travel away from the aperture, the relative strength of their amplitudes remains unaltered.

APPENDIX 3-A

For the Klein-Gordon fields propagating in dispersive media, we cannot use the "time-retarded" Kirchhoff-Huygens formula given by [cf. Eq. (2.2.4)]

$$\Psi(\mathbf{r},t)=\frac{1}{4\pi}\iint_S dS\left\{[\Psi]\frac{\partial}{\partial n}\left(\frac{1}{R}\right)-\frac{c}{R}\frac{\partial R}{\partial n}\left[\frac{\partial\Psi}{\partial n}\right]-\frac{1}{R}\left[\frac{\partial\Psi}{\partial n}\right]\right\}, \tag{3-A.1}$$

where the square brackets give the time-retarded values (at $t-R/c$) of the enclosed quantities. The variable *n* is the normal to the surface *S*, while *R* is the distance from the observation point to source points situated on the surface *S*. The main reason for not being able to use the formula given in (3-A.1) is that for dispersive waves the speeds of the various spectral components change with frequency. Hence, a single retarded time cannot be deduced from the inverse Fourier transform arising in the usual derivation of expression (3-A.1). To calculate the outgoing Klein-Gordon field propagating into the $z>0$ half space, one can start with Green's theorem [142]. This theorem states that for two functions Φ and Φ' that are well behaved and possess continuous first and second order derivatives, one has

$$\iiint_V dV\left\{\Phi\nabla^2\Phi'-\Phi'\nabla^2\Phi\right\}=\oiint_S dS\left\{\Phi\frac{\partial\Phi'}{\partial n}-\Phi'\frac{\partial\Phi}{\partial n}\right\}. \tag{3-A.2}$$

In the above expression Φ may be taken as the spectral amplitude of a Fourier superposition of sinusoidal solutions, viz.,

$$\hat{\Psi}(\mathbf{r},t)=\frac{1}{2\pi}\int_{-\infty}^{+\infty}d\omega\,\Phi(\mathbf{r},\omega)e^{i\omega t}. \tag{3-A.3}$$

The Klein-Gordon spectral components obey the following equation:

$$\left[\nabla^2+(\omega/c)^2-k_p^2\right]\Phi(\mathbf{r},\omega)=0. \tag{3-A.4}$$

If we choose Φ' also to be a solution of the above equation, then the left hand side of Eq. (3-A.2) becomes equal to zero; specifically,

$$\oiint_S dS\left\{\Phi\frac{\partial\Phi'}{\partial n}-\Phi'\frac{\partial\Phi}{\partial n}\right\}=0\,. \tag{3-A.5}$$

Choosing Φ' as

$$\Phi'(\mathbf{r},\omega)=\frac{e^{-i\kappa R}}{\kappa R}, \tag{3-A.6}$$

where $\kappa=\sqrt{(\omega/c)^2-k_p^2}$, and following the same derivation presented in section 8.3.1 in Ref. [152], the spectral amplitude at the observation point P is given by

$$\Phi(\mathbf{r}_p,\omega)=\frac{1}{4\pi}\iint_S dS\left\{\Phi\frac{\partial}{\partial n}\left(\frac{e^{-i\kappa R}}{R}\right)-\left(\frac{e^{-i\kappa R}}{R}\right)\frac{\partial\Phi}{\partial n}\right\}. \tag{3-A.7}$$

For the 3D scalar wave equation, substituting for Φ the inverse Fourier transform of $\hat{\Psi}(\mathbf{r},t)$ and using the dispersion relation $\omega=\kappa c,$ we arrive at the time-retarded Kirchhoff-Huygens formula given in Eq. (3-A.1). This is not possible, however, for the case of the Klein-Gordon equation because the dispersion relation becomes $\omega^2=\left(\kappa^2+k_p^2\right)c^2$. Consequently, the spectral components will have retarded times that depend on the respective frequencies. This should not be a problem for LW pulses since Eq. (3-A.7) can serve as a good starting point for deriving the radiated wavefields. Along these lines, we should note that we can substitute for Φ in Eq. (3-A.7) the temporal spectrum of the excitation wavefield of our flat dynamic aperture situated at $z = 0$; specifically,

$$\Phi_t(\rho,\omega)=\left[\int_0^\infty d\chi\chi J_0(\chi\rho)\Phi(\chi,\omega)e^{-i\sqrt{(\omega/c)^2-\chi^2-k_p^2}\,z}\right]_{z=0}. \tag{3-A.8}$$

Using this expression in conjunction with Eq. (3-A.7) and taking the inverse Fourier transform, we obtain

$$\Psi(\rho,z,t) = \Re\left\{\frac{1}{4\pi}\int_0^{2\pi} d\phi' \int_0^{\infty} d\rho'\, \rho' \left\{\frac{1}{2\pi}\int_0^{\infty} d\chi\chi\, J_0(\chi\rho)\int_0^{\infty} d\omega\, e^{i\omega t}\, \Phi(\chi,\omega)\right.\right.$$
$$\left.\left.\left(\frac{\partial}{\partial z'}\left(\frac{e^{-i\kappa R}}{R}\right)e^{-i\sqrt{\kappa^2-\chi^2}\,z'} - \frac{e^{-i\kappa R}}{R}\,\frac{\partial}{\partial z'}\left(e^{-i\sqrt{\kappa^2-\chi^2}\,z'}\right)\right)_{z'=0}\right\} \qquad \text{(3-A.9)}$$

In the above expression $R = \sqrt{\rho^2 + \rho'^2 - 2\rho\rho'\cos\phi' + (z-z')^2}$, where in our case $z' = 0$. The primed coordinates refer to source points on the aperture, while the unprimed ones refer to the observation points in the $z > 0$ half space. It follows, then, that

$$\frac{\partial}{\partial z'}\left(\frac{e^{-i\kappa R}}{R}\right) = -\,\frac{\partial}{\partial z}\left(\frac{e^{-i\kappa R}}{R}\right). \qquad \text{(3-A.10)}$$

To evaluate the partial derivative we use the integral representation

$$\frac{e^{-i\kappa R}}{R} = \frac{1}{\pi}\int_0^{\infty} d\lambda \int_{-\infty}^{+\infty} dk_z\; \lambda\, J_0(\lambda\rho^*)\frac{e^{-ik_z z}}{k_z^2 - (\kappa^2 - \lambda^2)}. \qquad \text{(3-A.11)}$$

Here, $\rho^* = \sqrt{\rho'^2 + \rho^2 - 2\rho'\rho\cos\phi'}$ and the contour of integration in the complex k_z-plane is shown in Fig. 3.6. For $k_z \to \sqrt{\kappa^2 - \lambda^2}$ and $z > 0$, the contour of integration is closed in the lower half plane in order to ensure the integrability of Eq. (3-A.11). The contour integration over the closed path C (C1,C2) yields

$$\frac{e^{-i\kappa R}}{R} = -i\int_0^{\infty} d\lambda\, \lambda\, J_0(\lambda\rho^*)\,\frac{e^{-i\left(\sqrt{\kappa^2-\lambda^2}\right)z}}{\sqrt{\kappa^2-\lambda^2}}. \qquad \text{(3-A.12)}$$

Keeping in mind the relation (3-A.10), the partial derivative with respect to z' gives

$$\frac{\partial}{\partial z'}\left(\frac{e^{-i\kappa R}}{R}\right) e^{-i\left(\sqrt{\kappa^2-\lambda^2}\right)z'}\Bigg|_{z'=0} = \int_0^\infty d\lambda\, \lambda\, J_0\left(\lambda\rho^*\right) e^{-i\left(\sqrt{\kappa^2-\lambda^2}\right)z} \quad . \tag{3-A.13}$$

.

Since λ is an integration variable, we may interchange it with χ, especially because of our prior knowledge of the appearance of the $\delta(\lambda-\chi)$ term when Eq. (3-A.7) is evaluated. Using Eq. (3-A.12), the second bracketed term in Eq. (3-A.9) becomes

$$-\frac{e^{-i\kappa R}}{R}\frac{\partial}{\partial z'}\left(e^{-i\left(\sqrt{\kappa^2-\lambda^2}\right)z'}\right)\Bigg|_{z'=0} = \int_0^\infty d\lambda\, \lambda\, J_0\left(\lambda\rho^*\right) e^{-i\left(\sqrt{\kappa^2-\lambda^2}\right)z} \quad . \tag{3-A.14}$$

.

The substitution of the two expressions given in Eqs. (3-A.13) and (3-A.14) reduces Eq. (3-A.9) to

$$\Psi(\rho,z,t) = \Re\left\{\frac{1}{4\pi^2}\int_0^{2\pi} d\phi' \int_0^\infty d\rho'\, \rho' \int_0^\infty d\chi\chi\, J_0(\chi\rho') \int_0^\infty d\omega\, e^{i\omega t}\, \Phi(\chi,\omega) \int_0^\infty d\lambda\lambda J_0\left(\lambda\rho^*\right) e^{-i\sqrt{(\omega/c)^2-\lambda^2-k_p^2}\,z}\right\}. \tag{3-A.15}$$

Making use of the addition theorem of Bessel functions [145], the integration over ϕ' can be carried out, yielding

$$\int_0^{2\pi} d\varphi'\, J_0\left(\lambda\left(\rho^2+\rho'^2-2\rho\rho'\cos\phi'\right)^{1/2}\right) = \sum_{m=-\infty}^{+\infty} J_m(\lambda\rho)\, J_m(\lambda\rho') \int_0^{2\pi} d\phi'\, e^{im\phi'} = 2\pi\, J_0(\lambda\rho)\, J_0(\lambda\rho'). \tag{3-A.16}$$

The radiated field, thus, becomes

$$\Psi(\rho,z,t)=\Re\left\{\frac{1}{2\pi}\int_0^\infty d\rho'\,\rho'\int_0^\infty d\chi\,\chi\,J_0(\chi\rho')\int_0^\infty d\omega\,\Phi(\chi,\omega)\,e^{i\omega t}\right.$$

$$\left.\times\int_0^\infty d\lambda\,\lambda\,J_0(\lambda\rho)\,J_0(\lambda\rho')\,e^{-i\left(\sqrt{(\omega/c)^2-\lambda^2-k_p^2}\right)z}\right\}. \tag{3-A.17}$$

The integration over ρ' can be evaluated using the orthogonality property of the Bessel functions [145] which gives a $\delta(\lambda-\chi)$ term. Thus, the integration over ρ' and λ reduces Eq. (3-A.17) to

$$\Psi(\rho,z,t)=\Re\left\{\frac{1}{2\pi}\int_0^\infty d\chi\,\chi\,J_0(\chi\rho)\int_0^\infty d\omega\,\Phi(\chi,\omega)\,e^{i\omega t}\,e^{-i\left(\sqrt{(\omega/c)^2-\chi^2-k_p^2}\right)z}d\omega\right\}. \tag{3-A.18}$$

This is the required result used in Sec.3.2 to calculate the decay rate of the centroid of the radiated Klein-Gordon LW pulse.

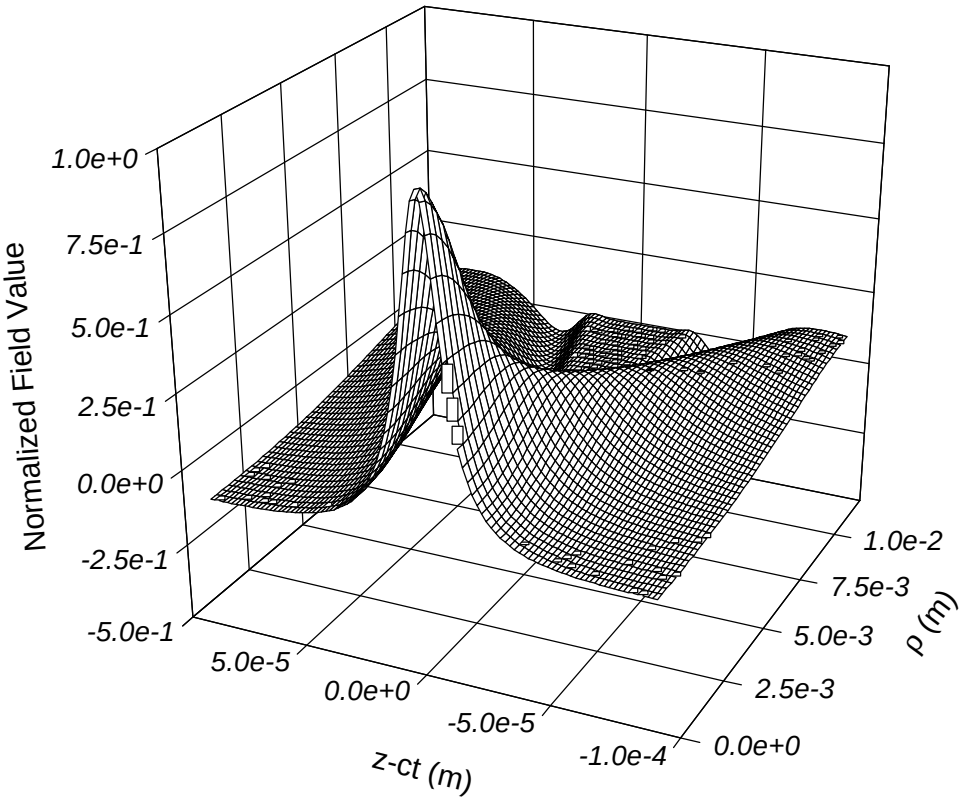

Figure 3.1a: The infinite aperture FWM pulse propagating in a dispersive medium characterized by the plasma frequency $f_p = 10$ GHz at $z = 236.25$ m and $k_s = k_p$.

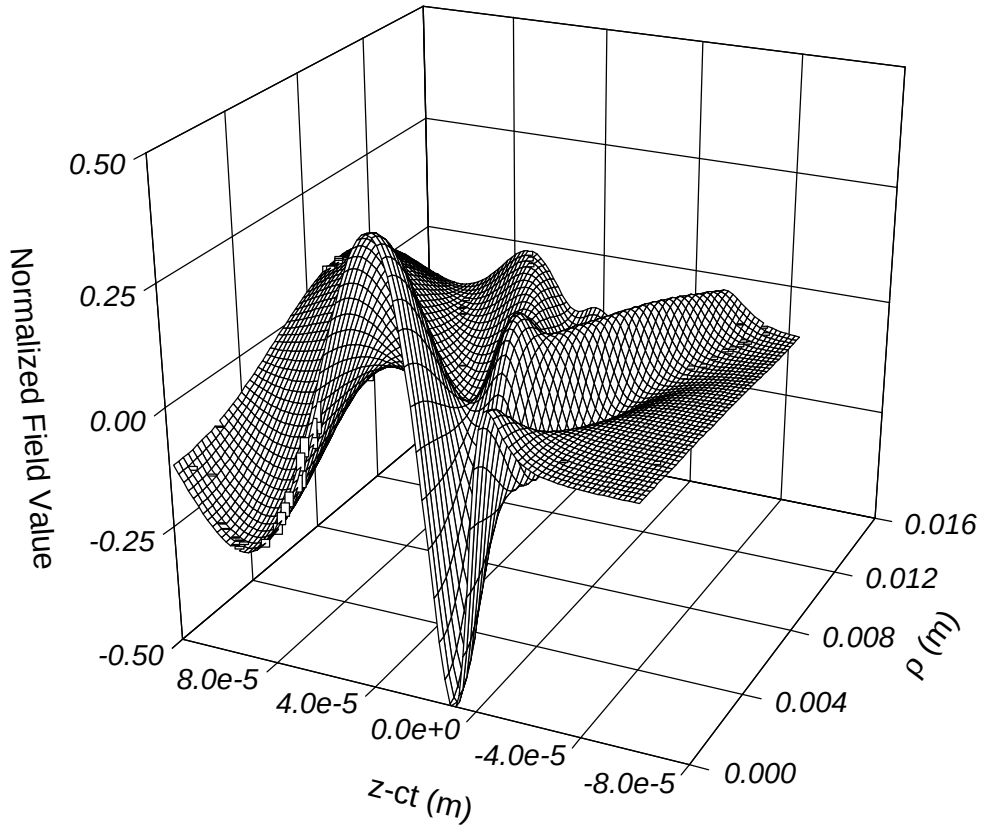

Figure 3.1b: The infinite aperture FWM pulse propagating in a dispersive medium characterized by the plasma frequency $f_p = 10$ GHz at $z = 236.25$ m and $k_s = 1.02k_p$.

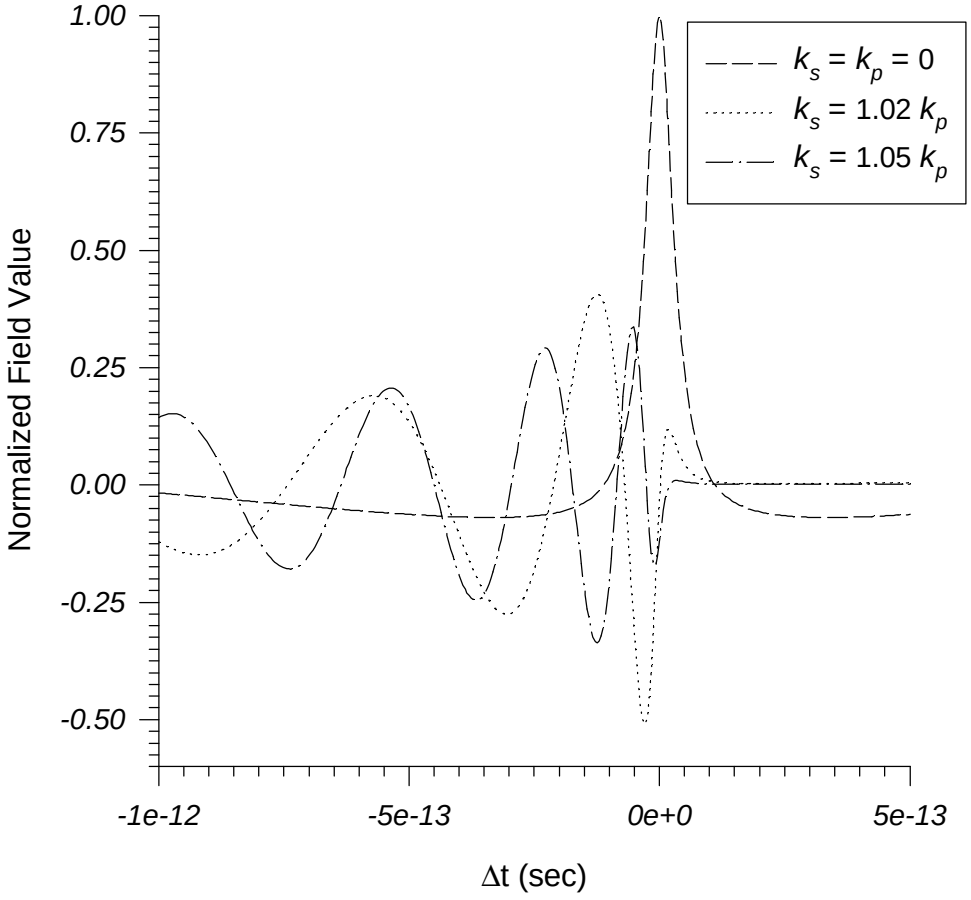

Figure 3.2: The time history of an infinite aperture FWM pulse propagating in a dispersive medium; $f_p = 10$ GHz, $k_s = k_p$, $1.02k_p$, $1.05k_p$ and $z = 236.25$ m.

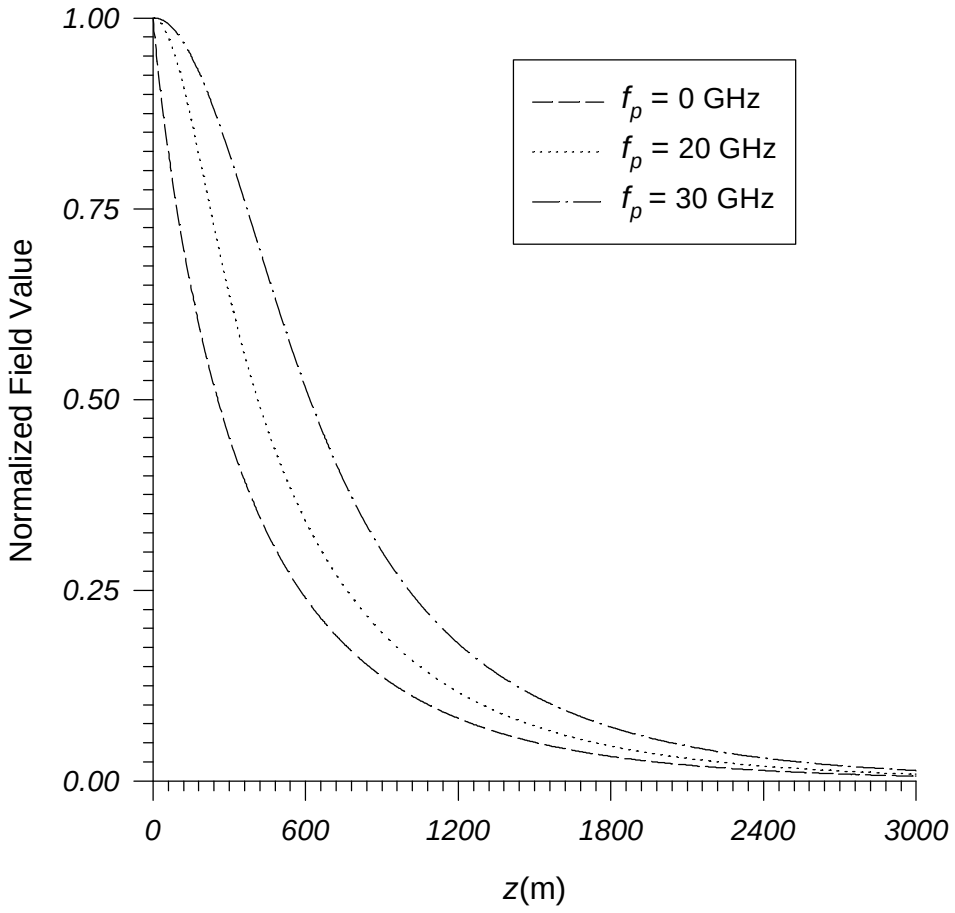

Figure 3.3: The decay of the amplitude of the centroid of the finite time FWM pulse for different plasma frequencies.

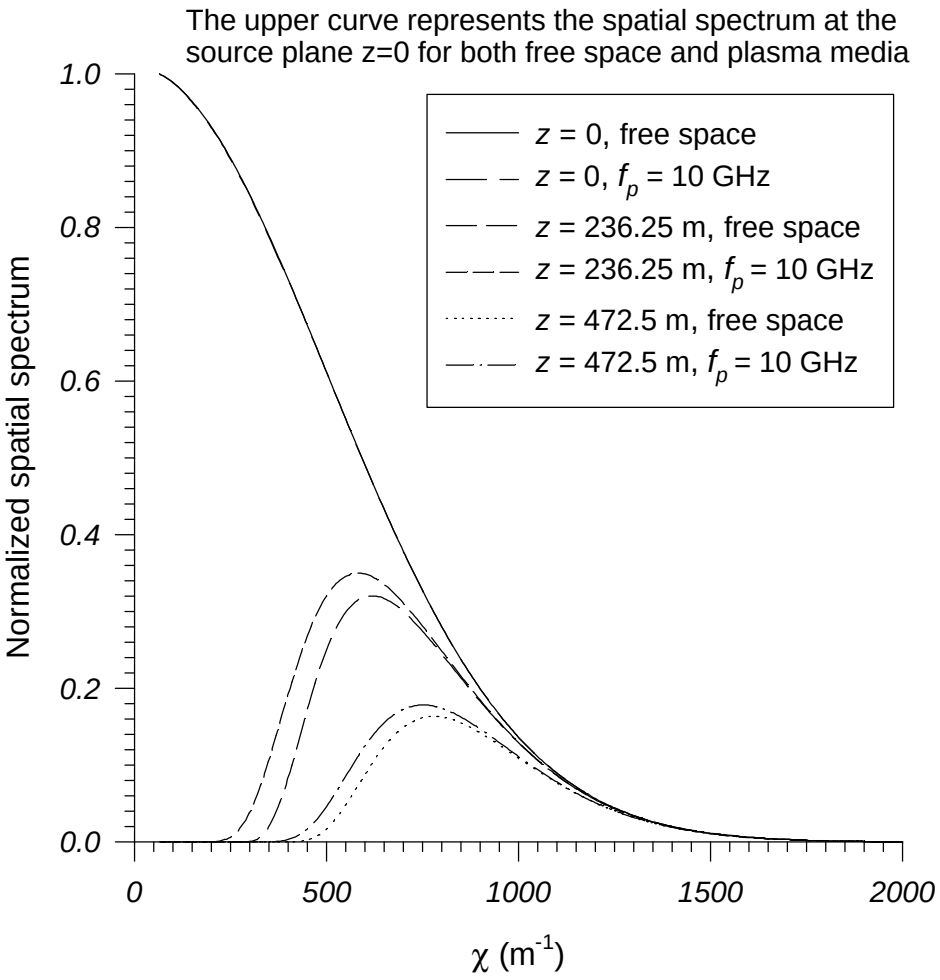

Figure 3.4a: The depletion of the spatial spectrum at different positions. The free space case is compared to a plasma medium having $f_p = 10$ GHz.

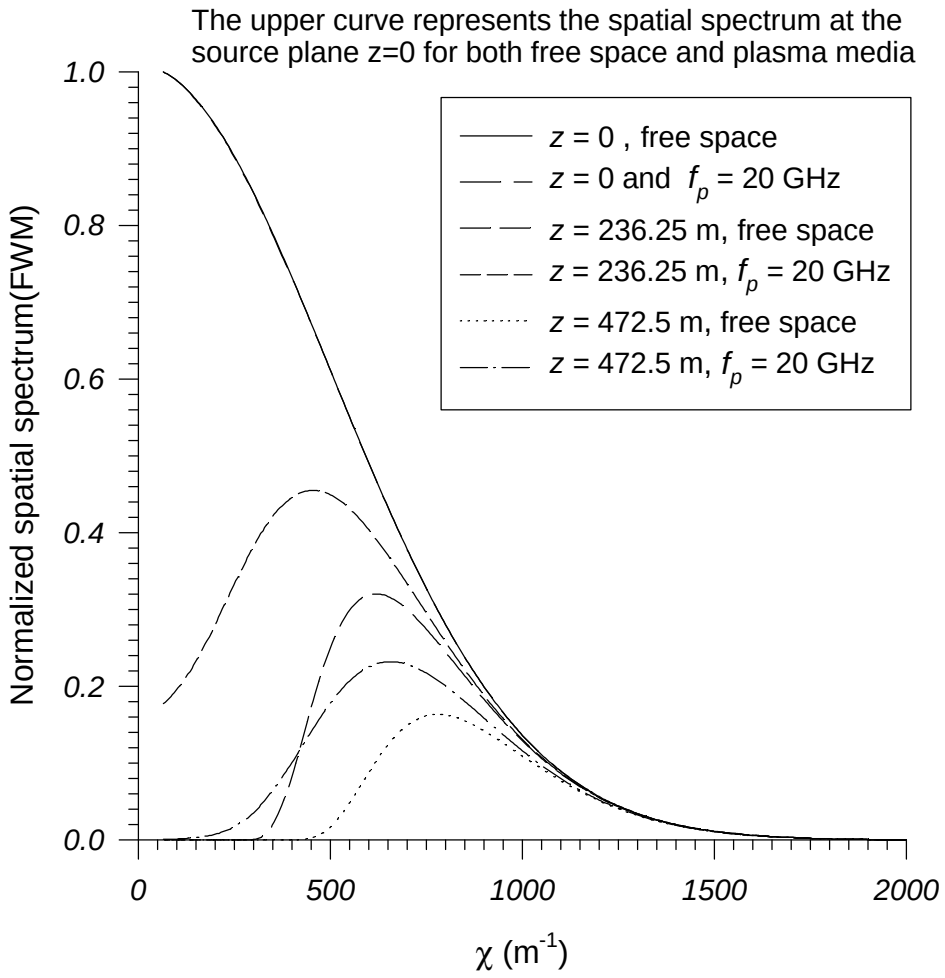

Figure 3.4b: The depletion of the spatial spectrum at different positions. The free space case is compared to a plasma medium having $f_p = 20$ GHz.

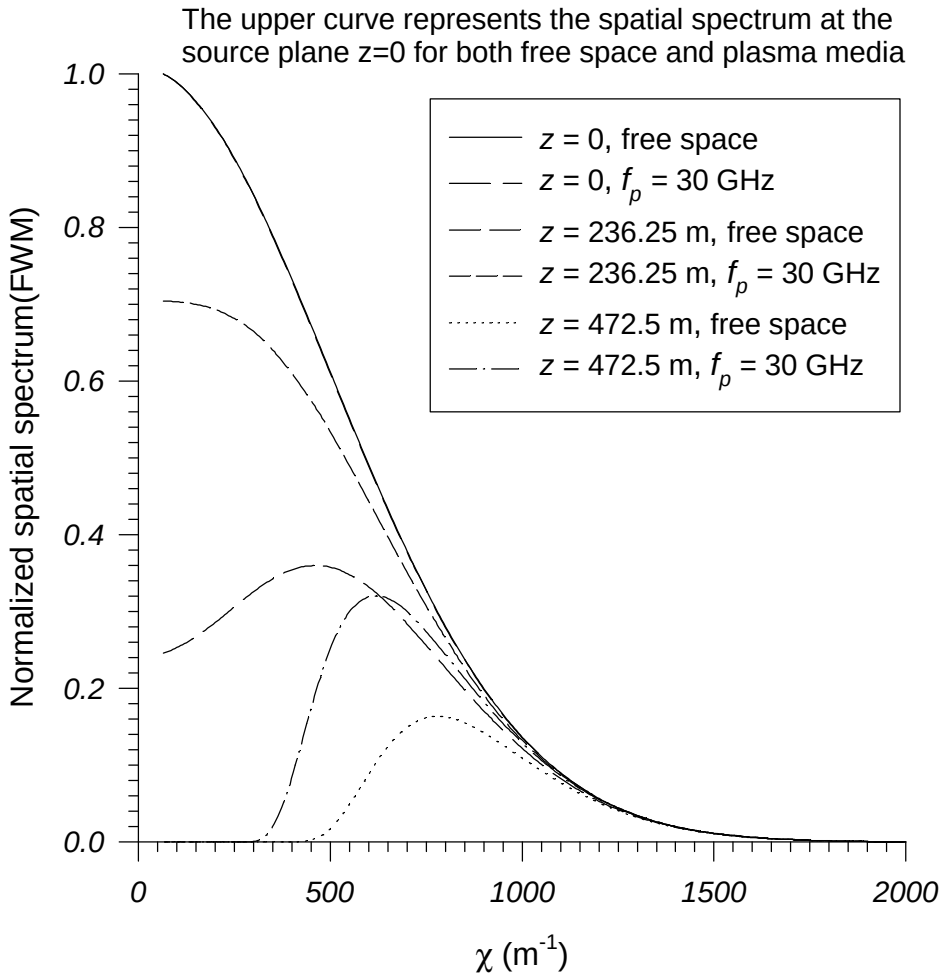

Figure 3.4c: The depletion of the spatial spectrum at different positions. The free space case is compared to a plasma medium having $f_p = 30$ GHz.

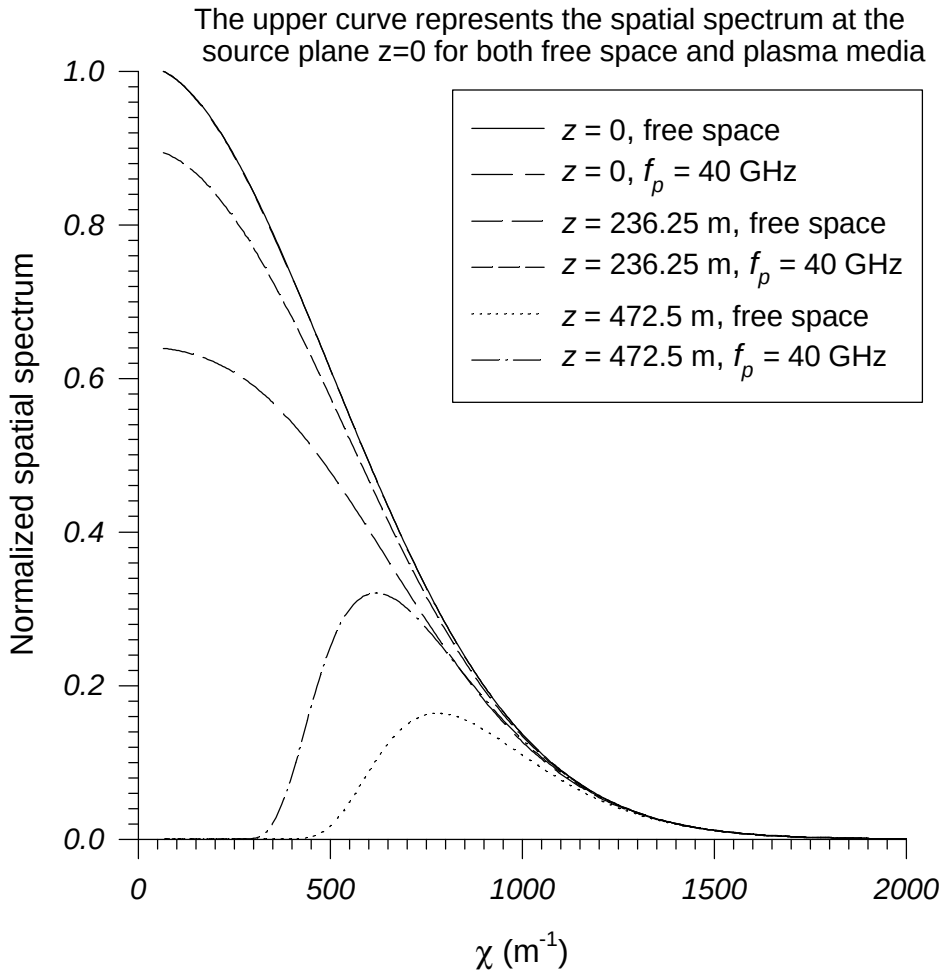

Figure 3.4d: The depletion of the spatial spectrum at different positions. The free space case is compared to a plasma medium having $f_p = 40$ GHz.

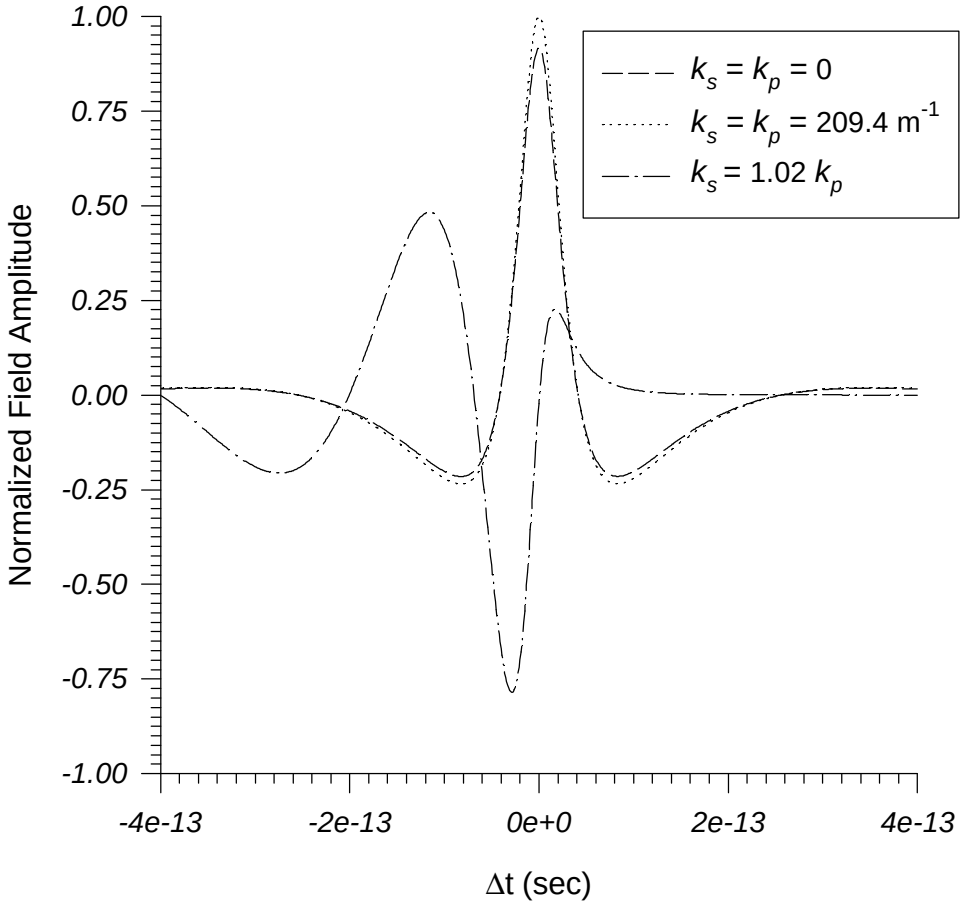

Figure 3.5a: A comparison of the time history of the finite-time FWM pulse propagating in free space as well as a dispersive medium; f_p = 10 GHz at z = 236.25 m

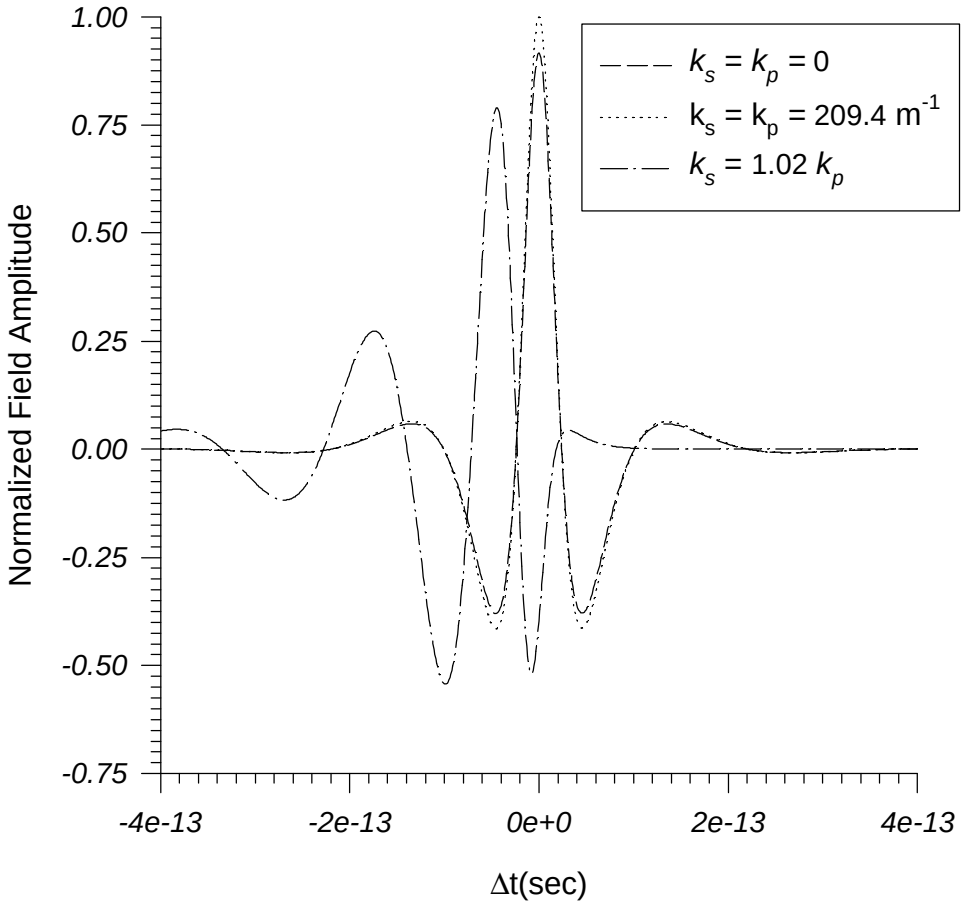

Figure 3.5b: A comparison of the time history of the finite-time FWM pulse propagating in free space as well as a dispersive medium; $f_p = 10$ GHz at $z = 708.74$ m .

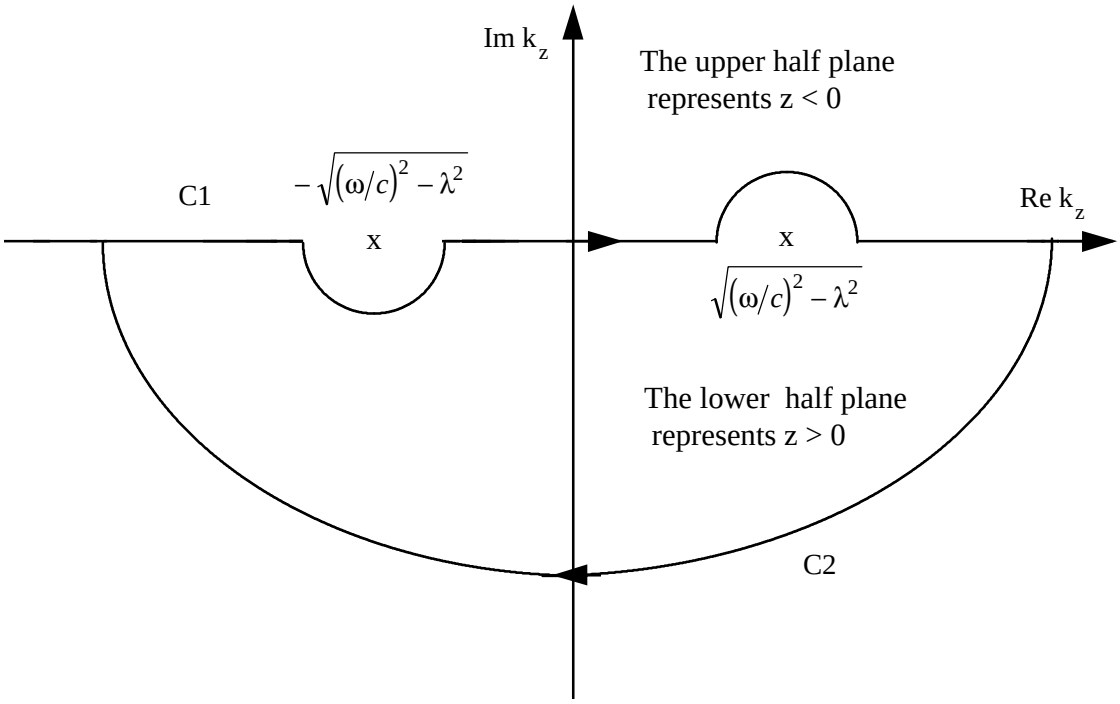

Figure 3.6: The contour used to evaluate the integration in Eq.(3-A.11)